Jurnal2019b

by Muhamad Jurnal

Submission date: 02-Apr-2021 02:47PM (UTC+0700)
Submission ID: 1548884981
File name: Ill_s2019_Article_FacingThePeatCO2ThreatDigitalM.pdf (7.5M)
Word count: 7944
Character count: 41278

Journal of Soils and Sediments
https://doi.org/10.1007/s11368-019-02328-0

SOILS, SEC 1 • SOIL ORGANIC MATTER DYNAMICS AND NUTRIENT CYCLING • RESEARCH ARTICLE

Facing the peat CO_2 threat: digital mapping of Indonesian peatlands—a proposed methodology and its application

Gábor Illés[1] · Sigit Sutikno[2] · Gábor Szatmári[3] · Ari Sandhyavitri[2] · László Pásztor[3] · Agus Kristijono[4] · Gábor Molnár[5] · Muhamad Yusa[2] · Balázs Székely[6]

Received: 21 February 2019 / Accepted: 10 April 2019

Abstract

Purpose We conducted this project to develop a feasible method for mapping tropical peat lands of Bengkalis Island—as a test site—in Indonesia.

Materials and methods The method based on limited availability of field measurements and a wide range of remotely sensed spatial datasets like radar elevation product, MODIS, and Landsat imageries. We applied land use category based sampling to extend existing field data of peat thickness. New peat thickness data was collected by boring and simultaneous electrical resistivity tomography (ERT). Based on remotely sensed and field data sets, peat maps were compiled by simulated spatial annealing. Peat map statistics were derived after 500 runs including mean, median, minimum, maximum, and percentile values.

Results and discussion The resulted maps represent the limiting values of expected peat thickness using 90% confidence level. Results showed that ERT is suitable for determining peat layer thickness. Using independent samples, we found that peat thickness predictions tend to overestimate peat thickness by ca. 2 m in general.

Conclusions According to predictions, the peat volume of Bengkalis Island is estimated to be in the range of 3.28–3.58 km^3.

Keywords Data integration · Indonesia · Peat-mapping concept · Probabilistic approach · Sampling strategy

Responsible editor: Weixin Ding

Electronic supplementary material The online version of this article (https://doi.org/10.1007/s11368-019-02328-0) contains supplementary material, which is available to authorized users.

✉ Gábor Szatmári
szatmari@rissac.hu

[1] NARIC Forest Research Institute, Sárvár, Hungary

[2] Civil Engineering Department, University of Riau, Pekanbaru, Indonesia

[3] Centre for Agricultural Research, Hungarian Academy of Sciences, Department of Soil Mapping and Environmental Informatics, Institute for Soil Science and Agricultural Chemistry, Budapest, Hungary

[4] Badan Pengkajian dan Penerapatan Teknologi, Jakarta, Indonesia

[5] MTA-ELTE Geological, Geophysical and Space Science Research Group, Hungarian Academy of Sciences at Eötvös Loránd University, Budapest, Hungary

[6] Department of Geophysics and Space Science, Eötvös Loránd University, Budapest, Hungary

1 Introduction

Greenhouse gases (GHGs) are in the focus of current climate change research. Because of the magnitude of CO_2 emission rates, carbon dioxide is considered to be the most important component of GHG (Pachauri et al. 2015).

Plants build their body from atmospheric CO_2 through photosynthesis that largely controls the natural balance of CO_2 emission and uptake. Regarding trees, it is well known that roughly half of the timber is composed of carbon that comes from atmospheric CO_2 (Körner 2003; Martin and Thomas 2011; Thomas and Martin 2012). In the case of the so-called zonal vegetation types that develop under macro-climatic driving forces on average sites—excluding extreme soil conditions—carbon is stored for decades in living trees and shrubs (Dixon et al. 1994; Lal 2005; Thurner et al. 2014). Later as dead organic matter develops from living plants, the majority of carbon is released back to the atmosphere while the minority enriches the soil organic carbon pool (Baritz et al. 2010; Somogyi et al. 2013; Lawson et al. 2015).

Published online: 03 May 2019

This cycle of CO_2 has two engines to run: photosynthesis and mineralization.

Peatlands are important zones of carbon accumulation. Peat development takes place under anaerobic, waterlogged conditions (Gorham 1991; Franzén and Franzen 2006; Tamocai 2006). Constrained decomposition leads to the accumulation of dead organic matter. While anaerobic conditions dominate, peatlands function as carbon sinks by storing magnitudes higher amount of carbon than mineral soils. Peatlands of the permafrost region account for less than 20% of the global soil coverage, but they contain approximately 50% of below-ground carbon pools (Tamocai et al. 2009; Sjögersten et al. 2014; Kurnianto et al. 2015).

Indonesia's peatlands are found in the inter-tropical convergence zone with a wet season (5–6 months) and a dry season (4–5 months). Annual precipitation exceeds 3500 mm, average temperature in coastal regions is around 25 °C. Peatlands developed in the last 5000 years (Supardi at al. 1993) after sea level has gradually fallen to its current position (Page et al. 2006). Coastal lowland basins started to turn into freshwater swamps as the precipitation washed out seawater reducing the area of mangroves. On millennial time scale, significant peat belt developed in the coastal region of Southeast Asian islands in the shape of domes gridded by rivers and covered by swamp forests. The total area of Southeast Asian peatlands is assumed to cover ca. 250,000 km^2 (Morley 1981; Morley 2002). The maximum thickness of the peat layer may reach 20 m (Jaenicke et al. 2008).

The water regime dependency and concentrated carbon storage functionality raise peatlands into a very important position in the battle of mitigating CO_2 emission rates. Therefore, it is an evident interest to preserve peatlands and their carbon content instead of releasing it back to the atmosphere.

Preservation of tropical peatlands requires knowledge about their vulnerability (Turetsky et al. 2015). The termination of waterlogged conditions by drainage exposes dead organic material to oxidative conditions and quick decomposition freeing up considerable amount of CO_2 in a very short time. In extreme cases, the CO_2 release happens by peat fires when tens of square kilometers of peatland areas burn down (Kool et al. 2006; Putra et al. 2008). Quick decomposition after artificial or natural draining of peatlands therefore destroys peat carbon sinks speeding up climate change processes (Gaveau et al. 2014).

Due to their natural occurrence (water-rich, lowland locations) peatlands were always threatened by human landscape transformation mainly in order to gain more agricultural land for food production or for other industrial or agricultural use. As a consequence, the area of peatlands reduced drastically by the end of the twentieth century and the remainder of these site fragments are now under strict legal protection (Vasander et al. 2003).

For quite the same reasons (food production and industrial plant cultivation), Indonesia's peatlands were faced with the same threat in the last few decades: hundreds of thousands of hectares were turned into farmlands and plantations after draining the lowland areas. In many cases, land use and water regime changes ended in disastrous results: drained soil was largely destroyed in extensive peat fires (Kool et al. 2006; Gaveau et al. 2014; Hayasaka et al. 2014; Huijnen et al. 2016). Consequently, in case of peat fires, the land surface subsides several meters that in coastal position open the way in front of sea floods. Moreover, extended peat fires increase CO_2 emission of the region, and the smoke that covers the sky and the cities causes respiratory illnesses (Putra et al. 2008).

In the last two decades, Indonesia lost 10–15% of its peatland areas due to rapid decomposition and fires. Besides this loss, it is estimated that the CO_2 emission rate increased by at least 50% during the same period (Hirano et al. 2014). Currently, the weather modification technology has an important role for mitigation strategy of the peat fires during dry season Indonesia (Sandhyavitri et al. 2018).

Our main research objective was to find fast, cheap, and efficient ways of mapping peatland areas to help Indonesian authorities to decide on the appropriate measures for preserving peatlands. For this reason, we joined to the initiative, which was announced during COP 21 Conference Paris 2015 when the Indonesian Peat Prize was launched (http, 1). Within this framework, research groups made efforts to improve peat land mapping techniques (Rudiyanto et al. 2016, 2018). Our research findings are presented in this paper.

2 Methodology and data

2.1 The study area

The methodology of Fig. 1 was tested on a test site in Riau Province, Indonesia (Fig. 2). Bengkalis Island lying 10 km off the coast of Sumatra, along the southwest side of the Strait of Malacca, is characterized by many land use categories ranging from villages to closed forest stands. The 900 km^2 large island has a very low relief; its highest point is 13 m above sea level. According to Supardi at al. (1993), 665 km^2 of the island is covered by peat more than 1 m thick. The test site area is the eastern part of the island of about 522 km^2. Kembung River (flowing toward NE) and Silan River (heading toward SW) split the peat-covered area into distinct domains.

2.2 Geological and geomorphic setting of the study area

Owing to the equatorial position of Indonesia, a great multitude of geoscientific processes, influences, and factors play a

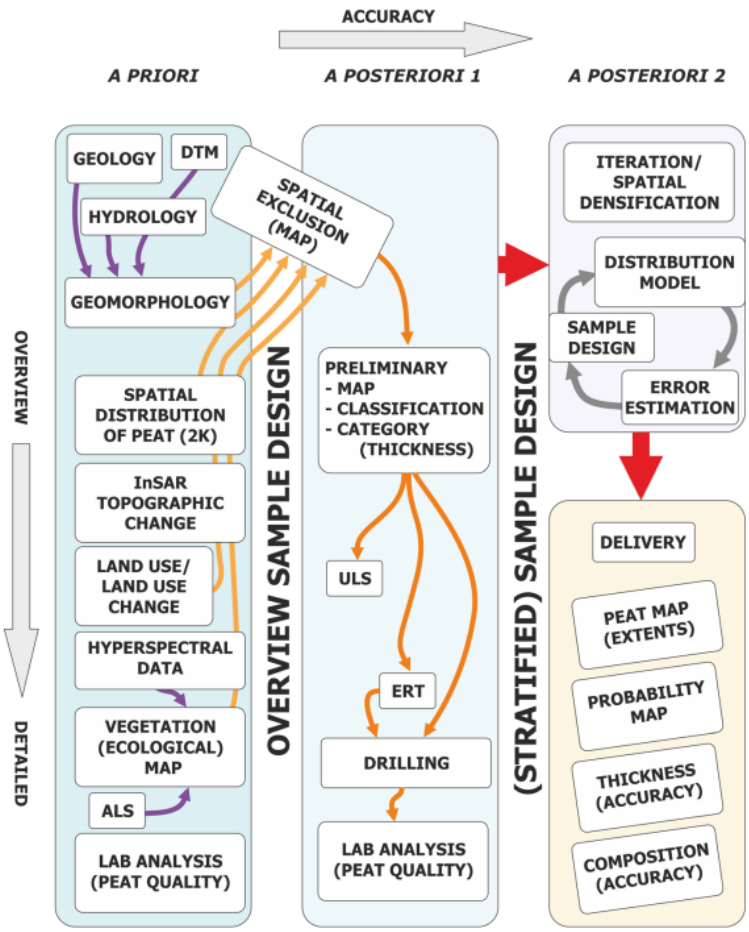

Fig. 1 The mapping and model development workflow

role in shaping the landscape. These processes may or may not contribute to the development of peat resources, or, on the contrary, may counteract of its preservation. In the widest sense, the interplay of the geomorphic–geological setting and the variation of the sea level have the general forcing effect on the resulting spatial distribution. These factors provide the potential environment for the development, but also may contribute to decay and complete disappearance of the raw material.

The back-arc position (in terms of plate tectonics) creates a wider belt of slow vertical crustal movements. It can manifest mostly in subsidence, but also uplift or slow-rate tilting at places, or even strike-slip faulting that also may have normal components (Katili 1970). The Strait of Malacca is one of these wider belts where the aforementioned differential uplift (that also may include subsidence) takes place. It is yet not very well known which of the two factors of the general sea-level changes or the differential subsidence controls the local (erosional) base level in this region. Volcanogenic influence (building-up and destruction of volcanic edifices) may contribute as flexural loading/unloading, potentially causing vertical displacements affecting wide areas hundreds of kilometers (see Cloetingh et al. 2007 for an extensive review). Other factors may also play a minor role, like centennial solar-terrestrial and tidal influence on sea level (see, e.g., Kázmér et al. 2008).

Geomorphological setting (driven by the underlying geological processes) determines the evolution of the local relief; both coastal floodplain scale and micro-geomorphological scale features are acting in peat accumulation and preservation or contributing to its decay. Low-relief islands are characterized by quite different sedimentological settings as larger island forelands: the latter environment may receive terrigenous material from upstream areas and may develop swampy conditions where redox circumstances may allow larger accumulation of organic material. On the other hand, the terrigenous influence of small, low-relief islands is restricted to the deposition of occasional wind-blown volcanic ash and the organic material accumulation is limited by the local biomass production. Furthermore, isolated smaller, low relief islands are more

Fig. 2 The test site location on Bengkalis Island (Indonesian Peat Prize documentation, IPP 2016)

influenced by the local and general sea-level oscillations. Due to the sea-level rise, many such islands have been decoupled from the general material transport conditions that determine the general pattern, developing local balance of accumulation of dead organic matter. It is also possible that this decoupling is a relatively new development; if this is the case, the provenance and age of the material should be studied in more detail.

2.3 Methodological approach and workflow

The approach presented here has an integrative character, as well as it is based on an iterative concept. The workflow follows these guidelines:

- Data sources are required that are generally available for thousands of square kilometers even if they are worse in quality than unique datasets available exclusively for unique sites.
- Freely available data should be integrated in order to keep the costs of mapping low, making the method economically applicable for other sites as well.
- The focus should be on reliable and widely accessible surveying methods that do not require too many additional investments and are available in general.
- We have to use non-destructive sampling methods for environmental reasons.

The workflow is presented in a flowchart in Fig. 1. The workflow consists of a package of initial data integration, and a two-phased package of data analysis and evaluation. The design and working out of the field measurements is based on the initial data in order to extend the dataset and verify the preliminary results. Field measurements are required partly for the mapping of spatial distribution of peat resources, partly to initialize the planning of peat sampling for those properties that can be measured only by sampling. The methodology works iteratively as every new piece of data initiates an evaluation of its contribution to error minimization and leads to recalculation of the sampling plan. The output of the flow is a series of maps of peat realizations, accuracy measures, and blind spot identification.

2.4 Data integration and compilation of preliminary maps

The organizers of the Indonesian Peat Prize defined a test area on Bengkalis Island and provided us with the major part of the initial dataset (http, 1). This spatial dataset contained several required items from Fig. 1. Among others, this initial dataset

Table 1 Landsat images and composites used in land use change assessments

Acquisition date	Spacecraft	Generated RGB composites	NDVI	NDII
1972-10-05	Landsat 1	NIR, R, G	Yes	No
1990-08-22	Landsat 5	Bands 6-7-2; 7-4-1; 7-4-5	Yes	Yes
1996-06-19	Landsat 5	Bands 6-7-2; 7-4-1; 7-4-5	Yes	Yes
1998-07-27	Landsat 5	Bands 6-7-2; 7-4-1; 7-4-5	Yes	Yes
2001-07-03	Landsat 5	Bands 6-7-2; 7-4-1; 7-4-5	Yes	Yes
2007-02-10	Landsat 5	Bands 6-7-2; 7-4-1; 7-4-5	Yes	Yes
2010-02-02	Landsat 5	Bands 6-7-2; 7-4-1; 7-4-5	Yes	Yes
2015-07-10	Landsat 8	Bands 10-7-3; 7-5-1; 7-5-6	Yes	Yes

contained a set of sampling points and peat map polygons that held information on peat thickness based on legacy data and on samples of 117 locations of the test site from earlier surveys. This existing sampling network served as the basis for the optimization of sampling design and spatial densification according to the data processing phase (Fig. 1).

In general, a countrywide digital terrain model (DTM) in a resolution and quality of the desired peat map series is needed; otherwise, the options of digital mapping solutions will be constrained. As the a priori dataset did not contain a satisfying DTM, the dataset was extended with the high-resolution surface model of TanDEM-X project that we successfully applied for at the Deutsche Zentrum für Luft- und Raumfahrt (DLR).

TanDEM-X provides high-resolution (12 m) radar-based land surface products that are available for the entire surface of Earth.

Being a radar-based dataset, the TanDEM-X data also has a DSM character, but this "issue" is compensated by the higher spatial resolution. For basic digital elevation product, we used the TanDEM-X elevation data with its error estimation.

The core of the used satellite database consisted of Landsat (http, 2) and MODIS products (http, 3). Finer resolution and long period of availability of Landsat images enabled us to produce detailed evaluations, while MODIS data delivered us standardized and well-developed earth data products. Using these imagery products, a desktop and online GIS database has been built (http, 4).

Concerning the high-resolution satellite imagery, 23 images can be found for the study area in Landsat database ranging between 1972 and 2015. Out of these 23, only 8 images have cloudless conditions that are suitable for land use (change) category assessment. The selected images are from the following years: 1972, 1990, 1996, 1998, 2001, 2007, 2010, and 2015. Table 1 summarizes the properties of the selected images. The selected band composites are suitable for distinguishing between vegetation types or soil surfaces (http, 5).

RGB composites, normalized difference vegetation index (NDVI; (NIR − RED)/(NIR + RED)) and normalized difference infrared index (NDII; (NIR − SWIR)/(NIR + SWIR); Hunt Jr and Rock 1989) have been calculated (Table 1). NDII index is very useful in the evaluation of drought and soil water deficit events (Sriwongsitanon et al. 2015).

The applied band combinations and calculated values are suitable for the evaluation of actual vegetation, to distinguish

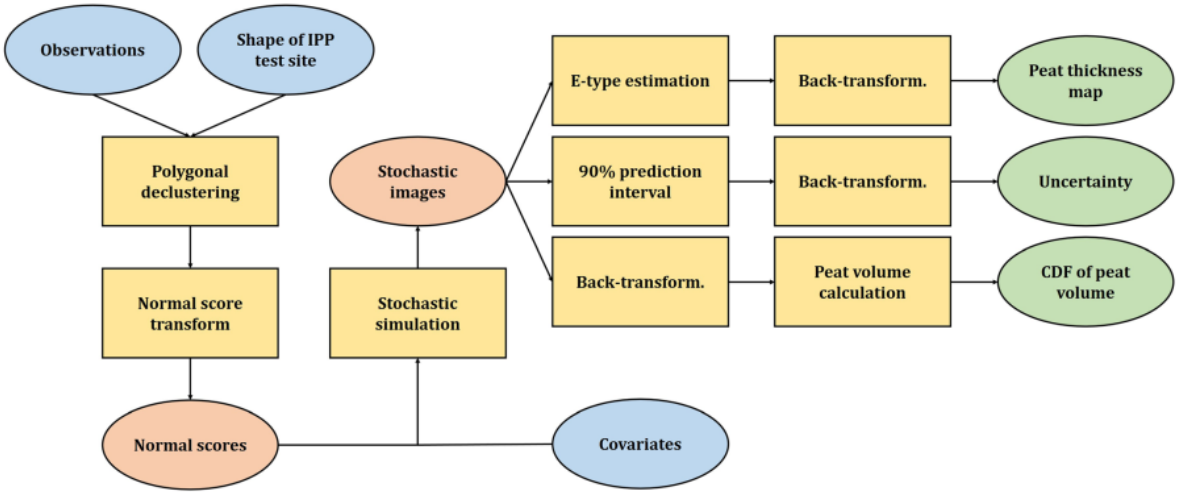

Fig. 3 Workflow of map compilation via sequential stochastic simulation

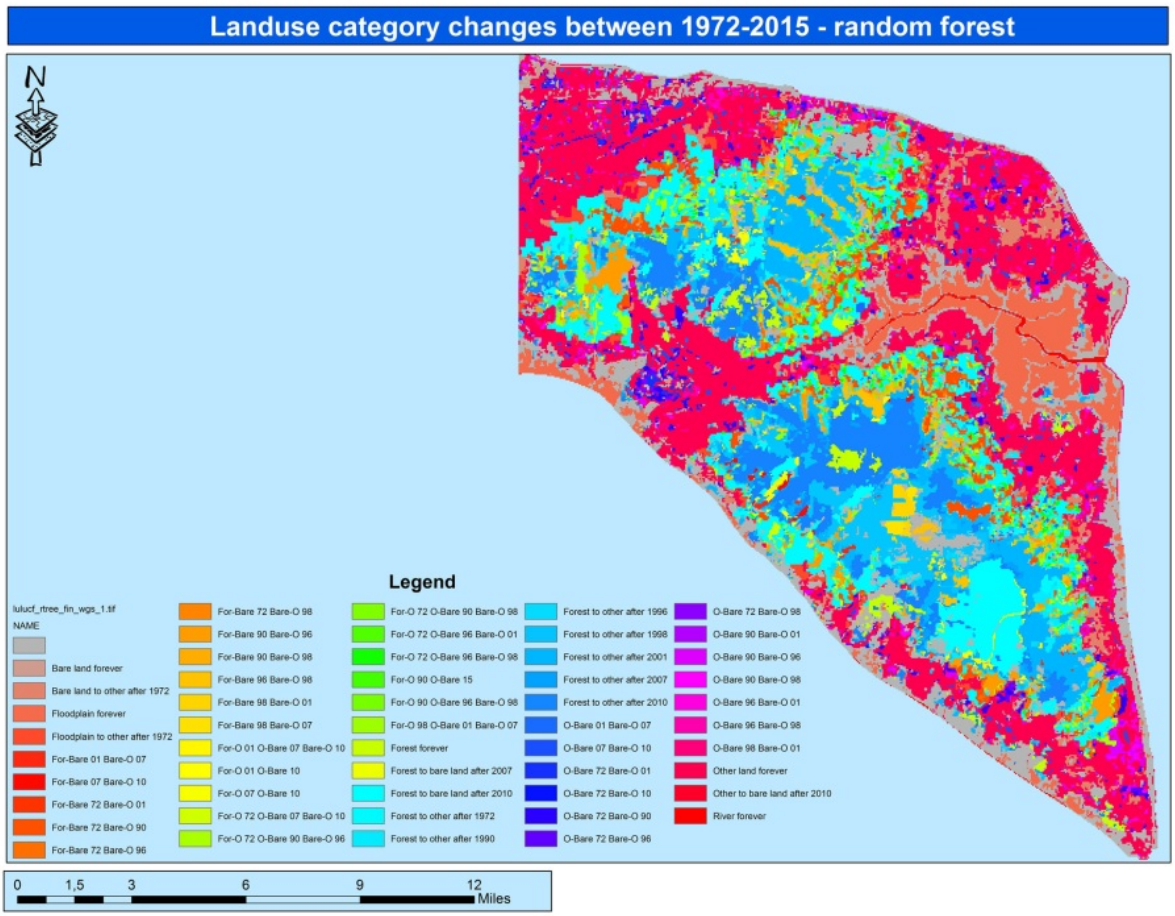

Fig. 4 Land use category changes on Bengkalis Island between 1972 and 2015 according to Random Forest classifier

between surface types (e.g., bare land, water, built areas) and to detect the temporal exchanges between land use categories (Mas et al. 2004; Ingram et al. 2005; Hwang et al. 2011).

Regarding MODIS, images from the period of 2000–2016 were used, applying the following products:

- MODIS EVI and NDVI products
- MODIS MOD9A1 products
- MODIS Fire products

Altogether, 769 images have been downloaded from NASA data server. The images were quality checked (including cloud cover), and only reliable pixels were used. The qualified image values were subject to standardization to make them comparable between years.

In order to detect peat fires, all data files for the study area having either the 8-day or 16-day returning period have been evaluated. For MODIS fire products, we involved only those pixels that were signed for high (9) or nominal (8) confidence levels of fires. MODIS NDVI and NDII index layers were also derived that were also subjects for quality check in order to involve only high-quality pixels.

2.4.1 Spatiotemporal land use change (LULUCF) analysis

Classified images were subjects of a spatiotemporal land use change (LULUCF) analysis. From Landsat data, we derived land cover maps over the period of 1972–2015. Land cover maps were also assigned to the dataset. They represented the land use changes and the conversion of forests into other land use forms.

The most relevant land use categories for each represented year have been identified and extracted via supervised image classification. Training areas for classes were selected manually in the way of visual image interpretation. For image segmentation and classification, eCognition Developer was used on the basis of training

Table 2 The summary of the field survey results (coordinates are according to WGS 1984 UTM Zone 48N; WKID 32648)

Number	Site	Coordinate *X*	Coordinate *Y*	Elevation (m)	Thickness (m) (from boring)	GWL depth (m)	Soil type	Von Post range
1	IPP-02A	165,528.70	197,063.71	7.31	4.00	0.8	Fibric Hemic	H2, H5
2	IPP-02	162,837.68	201,223.47	4.42	2.00	1.0	Fibric	H2, H3
3	IPP-03	165,662.82	199,970.74	6.79	6.00	0.3	Fibric Hemic	H2, H3, H4
4	IPP-04	160,548.49	206,181.43	4.32	2.50	0.4	Fibric	H2, H3
5	IPP-04A	156,805.85	202,206.75	2.10	0.10	0.3	Loam clay	–
6	IPP-06	164,948.85	206,044.79	9.15	2.50	0.4	Fibric	H2, H3
7	IPP-07	166,836.27	206,076.90	10.04	5.00	0.4	Fibric	H2, H3
8	IPP-09	164,148.83	209,973.19	4.67	4.40	0.3	Fibric Hemic	H2, H3, H6
9	IPP-10	169,536.15	209,715.59	4.10	6.00	0.4	Fibric Hemic	H1, H2, H3, H4, H5
10	IPP-10A	167,600.64	210,095.75	9.26	No information			
11	IPP-11	166,335.55	213,465.71	5.23	4.20	0.3	Fibric	H1, H2, H3
12	IPP-12	161,544.39	216,123.05	1.40	0.00	Tide	Clay	–
13	IPP-13	154,288.76	206,714.56	8.90	6.00	0.17	Fibric Hemic	H3, H4, H5, H6
14	IPP-14	154,587.00	206,982.70	8.87	7.50	0.03	Fibric Hemic	H3, H4, H5
15	IPP-21	155,879.70	215,046.53	8.11	7.00	0.5	Fibric Hemic	H2, H3, H4
16	IPP-22	155,419.00	217,782.95	0.58	0.00	0.3	Clay	–
17	IPP-23	156,383.37	217,817.99	0.52	0.00	0.1	Clay	–
18	IPP-25	148,820.11	213,695.71	10.43	More than 7 m	0.4	Fibric Hemic	H2, H3, H4
19	IPP-25A	147,314.18	213,133.87	9.24	6.20	0.3	Fibric Hemic	H2, H3
20	IPP-27	149,332.11	218,481.37	8.45	9.50	0.3	Fibric	H2, H3
21	IPP-29	148,284.02	218,946.65	9.25	9.00	0.17	Fibric	H2
22	IPP-30	146,326.60	220,530.41	6.39	6.00	1.3	Fibric Hemic	H2, H3, H4

areas and subsequent image layer data. For classification, the kNN and Random Forest classifiers were found to provide the best results. Accuracies based on samples were above 90%.

We combined the land cover layers into two single layers—one for the kNN classifier and one for the Random Forest classifier. The combined image was reclassified according to the data that "FROM what TO what" the land cover changed between "DATES" and "HOW MANY TIMES." For example, in this way, classes have been created like "Remained forest all the time" or "Forest converted to bare land after 1990," etc.

As a result, it became feasible to conduct a study on the land conversion process that took place in the island of Bengkalis. Consequently, it was possible to identify the approximate years when forests were converted into croplands or plantations.

These kinds of maps have a great importance in the interpretation of current extent and thickness of peat layers. The reason for this is nothing else than the different patches represent the major land units that had similar treatments in the past. Therefore, they are expected to be less diverse than surrounding areas regarding the thickness of peat or other properties.

2.4.2 Creating the preliminary peat map and sampling design

On the basis of the above-described GIS database, we were able to prepare preliminary peat maps and a starting sampling design for the examination of extended data collection, which could provide data for preparing second-stage maps.

For sampling optimization, we used the spatial simulated annealing (SSA) algorithm and the pre-survey

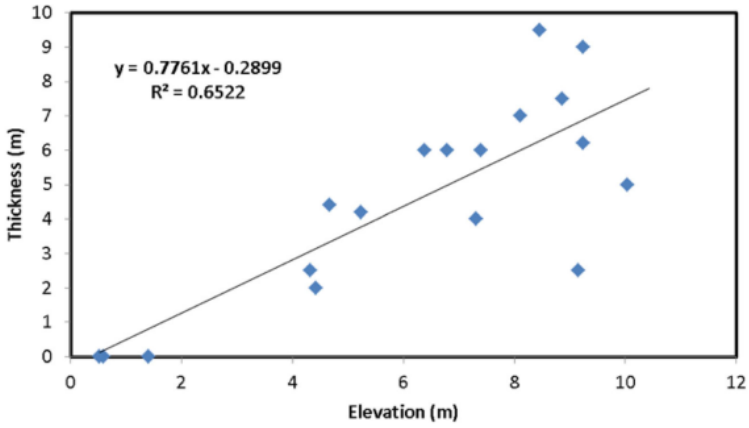

Fig. 5 Peat-dome thickness and elevation

quality measure that is the prediction variance of regression kriging.

During the optimization, we took into account the following covariates: fire occurrences, land use change maps, and principal components of NDVI and NDII maps. Existing sample point locations were also considered. Preliminary peat maps in the IPP Spatial Dataset were considered as weight layers in positive way.

We removed areas from optimization that are covered by artificial surfaces or water.

Changing the proposed sample size, we were able to make a calibration curve that shows the impact of sample size on pre-survey quality measure. This curve was used to define the number of necessary additional sample points. Neighborhood map shows the goodness of coverage and demonstrates spatial representativeness indicating suboptimal regions.

2.5 Field measurements

Besides the available field data, we carried out a data acquisition campaign in April 2017 assigned, at the locations determined by the optimized sampling design. Electrical resistivity tomography (ERT) measurements were combined with borehole sampling at designated sampling locations.

Multi-electrode surveying or resistivity tomography (ERT) is a direct current geophysical method based on Ohm's Law. A set of in-line ordered, equally spaced

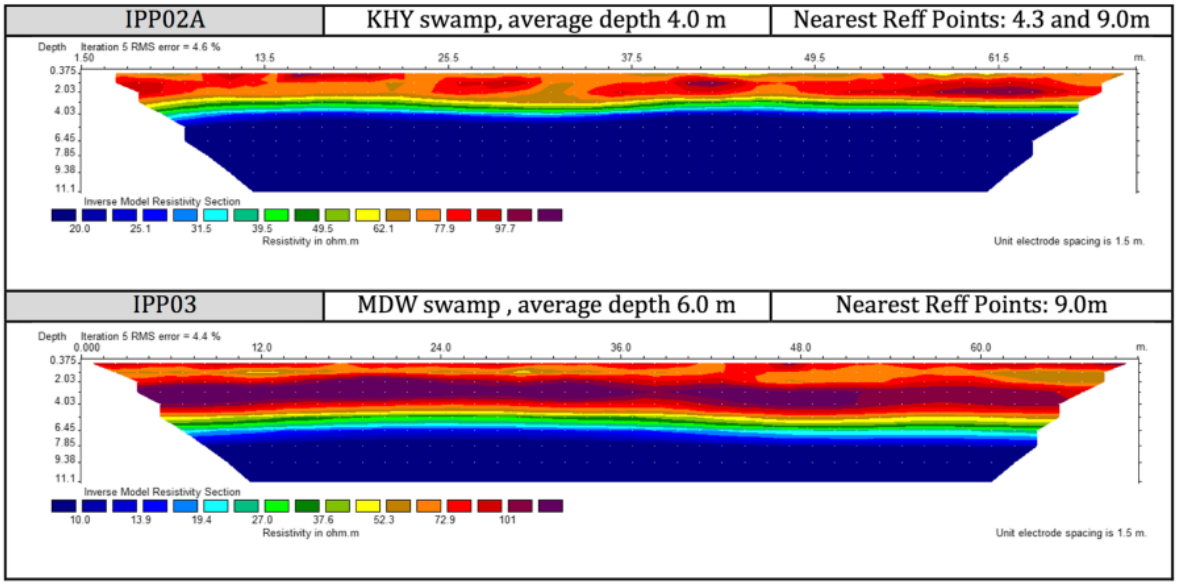

Fig. 6 2D Inverse model of below ground resistivity at ERT measurement points IPP2A (top) and IPP03 (bottom), showing 2D thickness of peat layer along the measurement transect (with is ca. 1.5× vertical exaggeration)

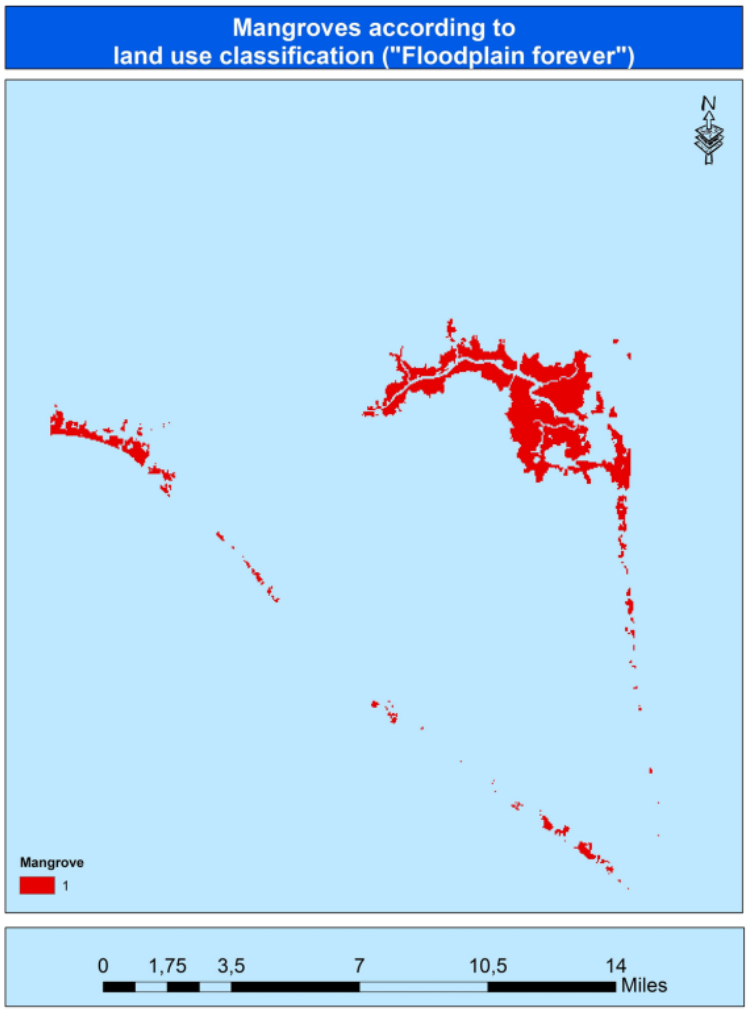

Fig. 7 Mangroves extracted from land use maps

electrodes are used to conduct current into the ground so that two of the electrodes serve as current input electrodes and the voltage is measured on other two electrodes. Considering the geometry (order of electrodes—which one is applied as a current, which one is a measuring electrode, and the distance between the electrodes), the apparent resistivity of the current-carrying ground is calculated. The four-electrode array moves through step-by-step all the electrodes providing many geometric configurations and resulting in many apparent resistivity of the respective ground below these electrodes. This set of apparent resistivity is then evaluated by geophysical inversion to get a 2D geometric distribution of the specific resistivity of the topsoil (Loke and Barker 1996).

The ERT measurements were carried out using ARES advance multi-channel automatic resistivity, manufactured by GF instrument. It mainly consists of transmitter and receiver. The transmitter has power up to 850 W, current up to 5 A (24-bit resolution), and voltage up to 2000 V, while the receiver has 10 channels, input voltage ± 20 V, and input impedance of 20 MW. The electrode spacing was 1.5 m with 48 electrodes.

Borehole sampling aimed the compilation of stratigraphic description for each point location of the additionally surveyed sites. These locations were used for accuracy assessment. Based on the degree of decomposition, every sample was classified according to the detailed classification of Von Post (1924), e.g., fibric (weakly decomposed), where the remnants of the decomposing wood/trunk is still identifiable along the very slightly decomposed wood/log/trunks. For shallow borehole sampling, a Jowsey improved peat sampler instrument was used (Jowsey 1966). Pictures were taken of every 50-cm sample section.

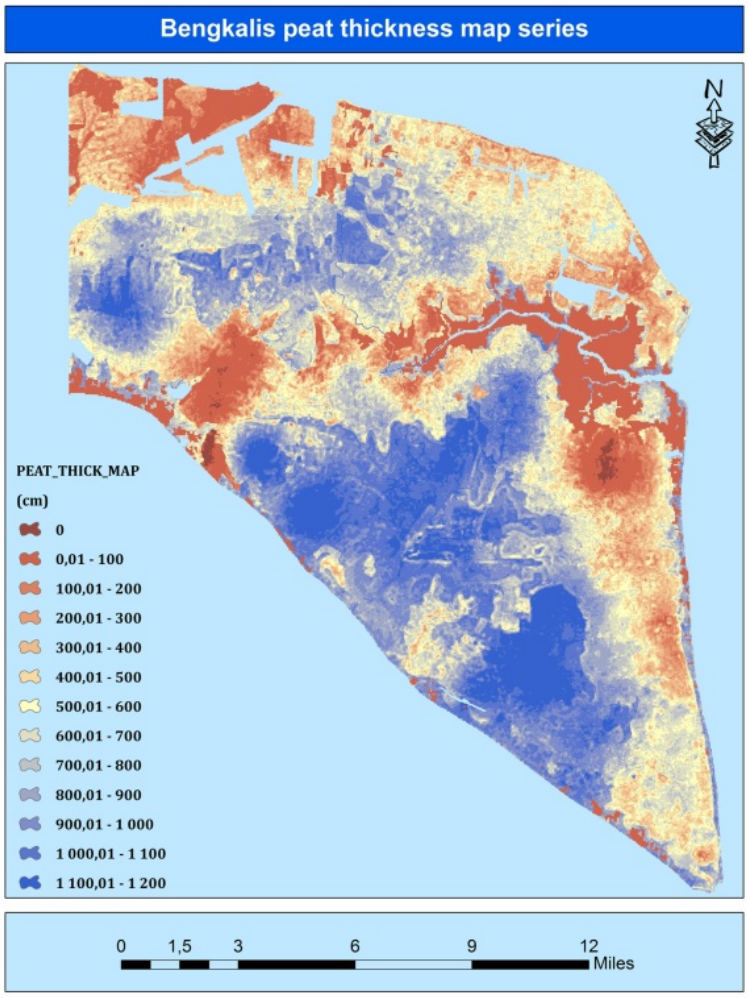

Fig. 8 The resulted map of sequential stochastic simulation with enclosed E-type simulation—average peat thickness

2.6 Methods of peat map compilation

2.6.1 Geostatistics

We applied a sequential Gaussian simulation algorithm (Goovaerts 1997) in which the mean and variance of the distribution function at each location were modeled by using regression kriging (Szatmári and Pásztor 2019). It can be used to generate alternative and equally probable realizations (so-called stochastic images) in order to model the spatial variability and uncertainty of peat thickness at IPP test site. The generated realizations reproduce the model statistics (e.g., sample histogram and variogram) and honor the input data (Szatmári et al. 2015). For this process, only the initial samples (i.e., 117 observations) were applied.

Figure 3 presents a flowchart on geostatistical techniques applied in this study. First of all, we applied a polygonal declustering technique because the peat thickness observations showed a clustered (or preferential) sampling scheme. Therefore, different weights were assigned to the data points based on their Voronoi's area proportion. These weights were used to compute the declustered sample histogram. In the next step, we applied normal score transform on the declustered histogram because sequential Gaussian simulation requires a multivariate normal space (Goovaerts 1997). We generated 500 alternative and equally probable stochastic images using the aforementioned simulation algorithm. The 500 realizations provide 500 simulated values for each pixel, which number is appropriate to compute the conditional cumulative distribution of peat thickness for each pixel. Using these cumulative distributions, the E-type estimation and the corresponding upper and lower bound of the 90% confidence interval were calculated for each pixel. Moreover, the 90% confidence interval's width was

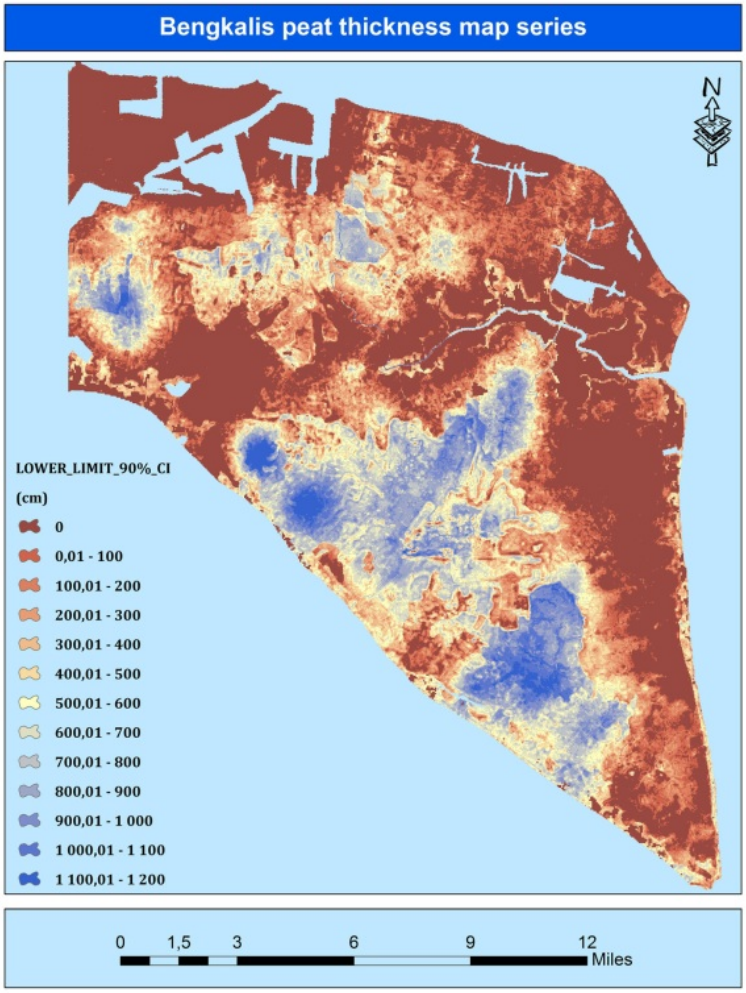

Fig. 9 The lower limit of 90% confidence interval for peat thickness according to sequential stochastic simulation

computed also, which provides a measure of the uncertainty, i.e., the wider the interval, the more uncertain the peat thickness estimation. The resulting maps were evaluated and compared to develop spatial variation and uncertainty measures by using the additionally collected samples during field works.

2.6.2 Excluding non-peat areas

The known mangrove areas had to be masked out as non-peat covered areas. From Landsat images using RED, NIR, and SWIR 1 bands, mangroves can be extracted before image processing takes place. The quotients of RED/SWIR 1 and SWIR 1/NIR distinguish between mangroves and other vegetation types (Long and Giri 2011; Noviar 2014). In fact, land use maps derived from Landsat data also offer a possible solution: areas classified as "Floodplain forever" in our land use categories practically cover all areas of mangrove vegetation.

3 Results

3.1 Results of LULUCF analysis

Due to the fact that the results of kNN and random forest classifiers were almost the same, we provide here only the random forest representation of land use changes over the studied periods. The summary map of land use category changes according to Random Forest classifier between 1972 and 2015 can be seen in Fig. 4. This map provides information on the rate of land use change processes in the last 43 years. The two main forest patches are obviously recognizable such as mangroves and other lands (shrubs). Differently colored patches within the borders

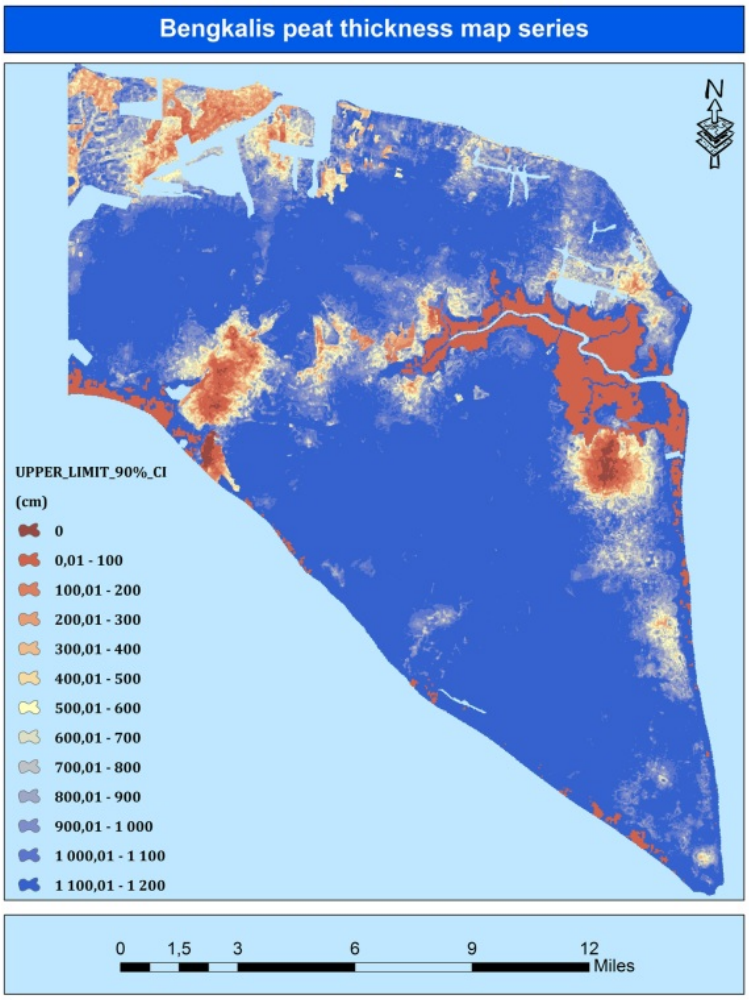

Fig. 10 The upper limit of 90% confidence interval for peat thickness according to sequential stochastic simulation

of bluish forest areas represent the temporal and spatial progress of land conversions from forests to other land types. Towards the inner part of historical woodlands, the size of the patches increases indicating the increasing spread of cultivation. Data shows that large areas were converted from forests into other categories between 2001 and 2010.

3.2 Results of additional sampling and ERT

Table 2 shows the summary of the field survey results of point locations. The data shows strong correlation between peat thickness and ground surface elevation as the peat forms low-relief peat domes. Figure 5 shows a linear fit between peat thickness and ground surface elevation. According to Fig. 5, elevation corresponds very well on peat thickness (domes).

Profiles of ERT measurements show parallel layered peat structures following soil surface. We found ERT suitable for mapping subsurface peat horizon. In the case of peat, the organic-rich (and also water-saturated) peat has significantly different resistivity value than that of the typical underlying bedrocks (clay respectively). Applying this method, the high resistivity contrast appearing on the inverted resistivity profile marks the bed of the peat (Fig. 6).

3.3 Exclusion of non-peat areas

As a further pre-processing step, areas can be defined (mangrove, tidal areas) using the RED, NIR, and SWIR 1 band calculations and land cover assessment that can be excluded from peat coverage maps. The resulted spatial exclusion map is shown in Fig. 7.

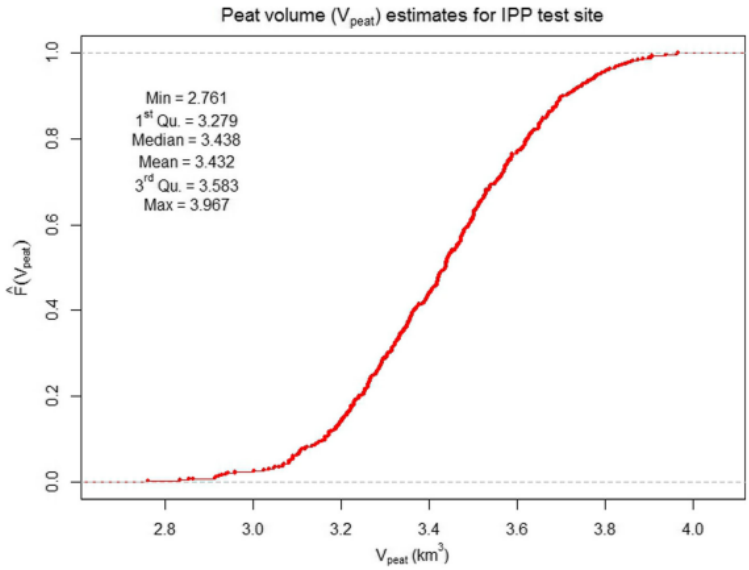

Fig. 11 Peat layer volume estimation curve according to SSA model

3.4 Resulted peat maps

As the results, we present here a series of maps that were obtained using the above-described method of peat map compilation in a 30-m resolution (Figs. 8–10). Figure 8 with sequential stochastic simulation results shows detailed peat map. The map represents the average values for every pixel calculated from the 500 simulations of peat surfaces.

Figure 9 represents the lower boundary of peat thickness using 90% confidence level. Blue areas indicate soils that must have significant peat deposits. Figure 10 represents the upper boundary of peat thickness using 90% confidence level. Red areas indicate soils that are not expected at all to have any peat deposits.

3.5 Estimation of peat volume

Our probabilistic approach allows a robust estimation of the peat volume. Of the 500 aforementioned stochastic images, a curve can be plotted: each simulation gives a peat volume; Fig. 11 is the cumulative distribution of the 500 actual volume values. Using Fig. 11, we are able to answer to an assessment question like this: How likely is it that the total volume of peat layer on Bengkalis Island is lower than 3.2 km^3? Although the predictions on peat thickness cover a relatively large range and have a great spatial variability on the edges of peat domes, because of the much less volume of peat in the shallower edges than in the inner part of peat domes, the overall peat volume estimation is much more robust. Both the mean and the median of the distribution is around 3.43 km^3 with an interquartile range of 0.31 km^3. In other words, the peat volume should be in the range of 3.28–3.58 km^3 with ca. 95% probability.

4 Discussion

Our results show that the a priori and a posteriori information integrated to a robust data model exhibit large spatial variations especially within the bracketing minima and maxima. These latter two properties (representing the extracted information content of the whole dataset) have relatively low undulations. This means that we could create a robust estimate for the upper and lower bracketing values. In terms of creating large-scale maps, this is one of the most important results. Concerning the peat thickness, the spatial undulations are relatively large as relatively high scatter occurs in the models. From the point of view of peat accumulation, but also (probably mostly) because of possible localized peat decay, there are almost no constraints for the lateral variation in the thickness: due to the interplay of deposition and decay from place to place, sharp changes are also possible in the real thickness values. In other words, the horizontal persistence of the peat thickness is relatively low.

The vegetation in the test area shows very strong anthropogenic effects (and so the original ecological pattern has been destroyed). This way, the remotely sensed data have been used in an environmental historical context (see above). It is a question to be studied whether this can be a widely applicable model or it has a local validity. This question arises from the fact that the cloudless images in

this area are very rare, and this way it is sometimes a question of luck which years can be covered by satellite imagery that can be integrated in the processing scheme.

Peat thickness maps of Fig. 8 and Fig. 11 correspond very well to the land use change maps that underline the importance of appropriate soil protection and the key role of human activity in peat thickness changes in the test area. Therefore, it is advisable to prepare land use category maps from retrospective data sets before mapping operations are taking place. This kind of even simplified LULUCF analysis is very useful for designing sampling schemes because areas in the same LULUCF categories are very likely to show similar impacts on their peat layer as a consequence of the similarity of human impacts. This does not mean of course the same or similar peat thickness by definition as it is influenced by more factors than human activity alone.

Regarding the results of other research groups working in Bengkalis with the same purpose (Rudiyanto et al. 2018), it can be stated that we came to slightly different results. Rudiyanto's team found that the total peat volume of Bengkalis is about 2.955 km^3. They characterized their estimation with a very narrow standard error (± 0.00062 km^3). Our results indicated that the mean value of total peat volume is about 3.432 km^3 while the mean standard error is 0.0101 km^3. This is a 16 times wider error range than what Rudiyanto's team has found.

Concerning accuracy assessment, we can imply on the basis of 22 independent samples that in the case of stochastic simulation-based model, the mean error of predictions was 2.1 m with standard deviation value of 3 m. Stochastic simulation slightly overestimated peat thickness of test site. In general, this method followed well the spatial pattern of peat thickness and peat dome occurrences. This error rate corresponds well to Rudiyanto's results reporting an RMSE between 1.8 and 2.8 m.

A major research question is that how far the lessons learned in this case history can be generalized for vast areas. Our assumption is (and actually our model works so) that the data density shows strong lateral changes. This is partly due to the nature of the phenomenon; partly it is caused by the inaccessibility or difficult to impossible measurement conditions. This can be expected for the whole area to be mapped.

We also expect that the input data will be clustered similarly as it is the case in the test site, so polygonal declustering has to be applied for other areas as well.

Of course, this reduces the accuracy of quick-look thickness values, but increases considerably the validity of bracketing probability value. This way, we can maximize the *local probabilities* of robust estimation. It is important to note that the regions characterized by different input data density are not to be compared with each other; only areas with similar observational spatial pattern should be compared.

It is also important to consider the economic aspects of the mapping and model development. The entire workflow can operate iteratively until the required result obtained or the allocated resources restrict the operation. Either way, this methodology helps to achieve the best results at any given financial level. Ultimately, in the case of using exclusively freely available datasets, this workflow generates only costs for data processing hours of experts. Additional expenses are generated only by field measurements (if there is no a priori information available for validation). From existing and newly measured samples, we were able to calculate the level of uncertainty at any given data density. Furthermore, the whole process is to be planned by balancing between cost and uncertainty measures.

5 Conclusions

Based on our studies using the Bengkalis data and the results of the field measurements and sampling, we can draw the following conclusions:

1. Although the vegetation analysis usually helps in detecting peat occurrences, in Indonesia this method can be used in areas that avoided considerable human impact (e.g., extensive plantation). In these cases, a retrospective, historical approach and detailed change analysis can replace the vegetation analysis.
2. As certain accumulation scenarios result in topographic undulations, it is crucial to have a relatively high-resolution, high-accuracy DTM that should be included in the modeling.
3. The volumetric estimates of peat layers can be robust, even if the peat layer thickness shows local undulations.
4. Differing hydrological, geomorphological, and geological conditions may require a revised model calculation including further geomorphometric inputs as well.
5. The economic feasibility of such surveys depends on the scalability of model using free of charge input data components.

Acknowledgements The authors are indebted to the Packard Foundation that made this study possible. We thank the close cooperation of the colleagues at the management of the Indonesian Peat Prize. The Deutsche Zentrum für Luft- und Raumfahrt (DLR) is thanked for providing free access to TanDEM-X data of the area (project ID DEM_FOREST1819). Colleagues and students carrying out the field measurements are thanked for their tedious work despite the hard field conditions.

Funding Information Open access funding provided by MTA Centre for Agricultural Research (MTA ATK).

References

Baritz R, Seufert G, Montanarella L, Van Ranst E (2010) Carbon concentrations and stocks in forest soils of Europe. For Ecol Manag 260: 262–277

Cloetingh SAPL, Ziegler PA, Bogaard PJF, Andriessen PAM, Artemieva IM, Bada G, van Balen RT, Beekman F, Ben-Avraham Z, Brun JP, Bunge HP, Burov EB, Carbonell R, Faccenna C, Friedrich A, Gallart J, Green AG, Heidbach O, Jones AG, Matenco L, Mosar J, Oncken O, Pascal C, Peters G, Sliaupa S, Soesoo A, Spakman W, Stephenson RA, Thybo H, Torsvik T, de Vicente G, Wenzel F, Wortel MJR (2007) TOPO-EUROPE: the geoscience of coupled deep earth-surface processes. Glob Planet Chang 58:1–118

Dixon RK, Solomon AM, Brown S, Houghton RA, Trexier MC, Wisniewski J (1994) Carbon pools and flux of global forest ecosystems. Science 263:185–190

Franzén LG, Franzen LG (2006) Increased decomposition of subsurface peat in Swedish raised bogs: are temperate peatlands still net sinks of carbon? Mires Peat 1:1–16

Gaveau DLA, Salim MA, Hergoualc'h K et al (2014) Major atmospheric emissions from peat fires in Southeast Asia during non-drought years: evidence from the 2013 Sumatran fires. Sci Rep 4. https://doi.org/10.1038/srep06112

Goovaerts P (1997) Geostatistics for natural resources evaluation. Oxford University Press

Gorham E (1991) Northern peatlands: role in the carbon cycle and probable responses to climatic warming. Ecol Appl 1:182–195

Hayasaka H, Noguchi I, Putra EI, Yulianti N, Vadrevu K (2014) Peat-fire-related air pollution in Central Kalimantan, Indonesia. Environ Pollut 195:257–266

Hirano T, Kusin K, Limin S, Osaki M (2014) Carbon dioxide emissions through oxidative peat decomposition on a burnt tropical peatland. Glob Chang Biol 20:555–565

Huijnen V, Wooster MJ, Kaiser JW, Gaveau DLA, Flemming J, Parrington M, Inness A, Murdiyarso D, Main B, van Weele M (2016) Fire carbon emissions over maritime Southeast Asia in 2015 largest since 1997. Sci Rep 6:1–8. https://doi.org/10.1038/srep26886

Hunt ER Jr, Rock BN (1989) Detection of changes in leaf water content using near- and middle-infrared reflectances. Remote Sens Environ 30:43–54

Hwang T, Song C, Bolstad PV, Band LE (2011) Downscaling real-time vegetation dynamics by fusing multi-temporal MODIS and Landsat NDVI in topographically complex terrain. Remote Sens Environ 115:2499–2512

Ingram JC, Dawson TP, Whittaker RJ (2005) Mapping tropical forest structure in southeastern Madagascar using remote sensing and artificial neural networks. Remote Sens Environ 94:491–507

Jaenicke J, Rieley JO, Mott C, Kimman P, Siegert F (2008) Determination of the amount of carbon stored in Indonesian peatlands. Geoderma 147:151–158

Jowsey PC (1966) An improved peat sampler. New Phytol 65:245–248

Katili JA (1970) Additional evidence of transcurrent faulting in Sumatra and Sulawesi. Bull Nat Inst Geol Min Bandung:15–28

Kázmér M, Oka S, Asami R, Yamada T, Iryu Y, Székely B (2008) Annual record of environmental history in corals and tree-rings—a land–sea correlation at Ogasawara Islands, Japan. Geophys Res Abstr 10: 05183

Kool DM, Buurman P, Hoekman DH (2006) Oxidation and compaction of a collapsed peat dome in Central Kalimantan. Geoderma 137: 217–225

Körner C (2003) Carbon limitation in trees. J Ecol 91:4–17

Kurnianto S, Warren M, Talbot J, Kauffman B, Murdiyarso D, Frolking S (2015) Carbon accumulation of tropical peatlands over millennia: a modeling approach. Glob Chang Biol 21:431–444

Lal R (2005) Forest soils and carbon sequestration. For Ecol Manag 220: 242–258

Lawson IT, Kelly TJ, Aplin P, Boom A, Dargie G, Draper FCH, Hassan PNZBP, Hoyos-Santillan J, Kaduk J, Large D, Murphy W, Page SE, Roucoux KH, Sjögersten S, Tansey K, Waldram M, Wedeux BMM, Wheeler J (2015) Improving estimates of tropical peatland area, carbon storage, and greenhouse gas fluxes. Wetl Ecol Manag 23:327–346

Loke MH, Barker RD (1996) Rapid least-squares inversion of apparent resistivity pseudosections by a quasi-Newton method1. Geophys Prospect 44:131–152

Long JB, Giri C (2011) Mapping the Philippines' mangrove forests using landsat imagery. Sensors 11(3):2972–2981. https://doi.org/10.3390/s110302972

Martin AR, Thomas SC (2011) A reassessment of carbon content in tropical trees. PLoS One 6:e23533. https://doi.org/10.1371/journal.pone.0023533

Mas JF, Puig H, Palacio JL, Sosa-López A (2004) Modelling deforestation using GIS and artificial neural networks. Environ Model Softw 19:461–471

Morley R (1981) Development and vegetation dynamics of a lowland ombrogenous peat swamp in Kalimantan Tengah, Indonesia. J Biogeogr 8:383–404

Morley CK (2002) A tectonic model for the tertiary evolution of strike-slip faults and rift basins in SE Asia. Tectonophysics 347:189–215

Noviar H (2014) Aplikasi data penginderaan jauh untuk inventarisasi hutan mangrove di kabupaten bengkalis propinsi riau. In: Hasyim K and Prasasti T (eds) Pemanfaatan Citra Penginderaan Jauh untuk Sumber Daya Wilayah Darat. Crestpen Press, Bogor, 85–94

Pachauri RK, Meyer L, Core-Writing-Team (2015) Climate Change 2014 Synthesis Report. Geneva

Page SE, Rieley JO, Wüst R (2006) Chapter 7 lowland tropical peatlands of Southeast Asia. Dev Earth Surf Process 9:145–172

Putra EI, Hayasaka H, Takahashi H, Usup A (2008) Recent peat fire activity in the mega rice project area, Central Kalimantan, Indonesia. J Disaster Res 3:1–6

Rudiyanto MB, Setiawan BI et al (2016) Digital mapping for cost-effective and accurate prediction of the depth and carbon stocks in Indonesian peatlands. Geoderma 272:20–31

Rudiyanto MB, Setiawan BI et al (2018) Open digital mapping as a cost-effective method for mapping peat thickness and assessing the carbon stock of tropical peatlands. Geoderma 313:25–40

Sandhyavitri A, Perdana MA, Sutikno S, Widodo FH (2018) The roles of weather modification technology in mitigation of the peat fires during a period of dry season in Bengkalis, Indonesia. IOP Conf Ser Mater Sci Eng 309:012016

Sjögersten S, Black CR, Evers S, Hoyos-Santillan J, Wright EL, Turner BL (2014) Tropical wetlands: a missing link in the global carbon cycle? Glob Biogeochem Cycles 28:1371–1386

Somogyi Z, Bidló A, Csiha I, Illés G (2013) Country-level carbon balance of forest soils: a country-specific model based on case studies in Hungary. Eur J For Res 132:825–840

Sriwongsitanon N, Gao H, Savenije HHG, Maekan E, Saengsawang S, Thianpopirug S (2015) The normalized difference infrared index

(NDII) as a proxy for soil moisture storage in hydrological modelling. Hydrol Earth Syst Sci Discuss 12:8419–8457
Supardi, Subekty AD, Neuzil SG (1993) General geology and peat resources of the Siak Kanan and Bengkalis Island peat deposits, Sumatra, Indonesia. In: Cobb JC and Cecil CB (eds) Modern and ancient coal-forming environments. Boulder, Colorado, Geological Society of America Special Paper 286, pp 45–62
Szatmári G, Pásztor L (2019) Comparison of various uncertainty modelling approaches based on geostatistics and machine learning algorithms. Geoderma 337:1329–1340
Szatmári G, Barta K, Farsang A, Pásztor L (2015) Testing a sequential stochastic simulation method based on regression kriging in a catchment area in southern Hungary. Geol Croat 68:273–283
Tamocai C, Canadell JG, Schuur EAG et al (2009) Soil organic carbon pools in the northern circumpolar permafrost region. Glob Biogeochem Cycles 23:1–11
Tamocai C (2006) The effect of climate change on carbon in Canadian peatlands. Glob Planet Chang 53:222–232
Thomas SC, Martin AR (2012) Carbon content of tree tissues: a synthesis. Forests 3:332–352
Thurner M, Beer C, Santoro M, Carvalhais N, Wutzler T, Schepaschenko D, Shvidenko A, Kompter E, Ahrens B, Levick SR, Schmullius C (2014) Carbon stock and density of northern boreal and temperate forests. Glob Ecol Biogeogr 23:297–310
Turetsky MR, Benscoter B, Page S, Rein G, van der Werf GR, Watts A (2015) Global vulnerability of peatlands to fire and carbon loss. Nat Geosci 8:11–14
Vasander H, Tuittila ES, Lode E et al (2003) Status and restoration of peatlands in northern Europe. In: Wetlands ecology and management, pp 51–63
Von Post L (1924) Das genetische System der organogenen Bildungen Schwedens. Memoires sur la nomenclature et la classification des sols. International Committee of Soil Science, Helsinki, pp 287–304

HTTP references

www.indonesianpeatprize.com
https://landsat.usgs.gov
https://modis.gsfc.nasa.gov
www.ertigis.hu/intranet/indonez.htm
https://landsat.usgs.gov/what-are-band-designations-landsat-satellites

Jurnal2019b

ORIGINALITY REPORT

3%	2%	3%	%
SIMILARITY INDEX	INTERNET SOURCES	PUBLICATIONS	STUDENT PAPERS

PRIMARY SOURCES

1	real.mtak.hu Internet Source	1%
2	Gábor Szatmári, Károly Barta, Andrea Farsang, László Pásztor. "Testing a sequential stochastic simulation method based on regression kriging in a catchment area in Southern Hungary", Geologia Croatica, 2015 Publication	1%
3	istina.msu.ru Internet Source	1%

Exclude quotes	On	Exclude matches	< 1%
Exclude bibliography	On		